Journal of Sound and Vibration (1999) **226**(1), 101–123
Article No. jsvi.1999.2278, available online at http://www.idealibrary.com on IDEAL®

VIBROACOUSTIC ANALYSIS OF A FINITE CYLINDRICAL SHELL WITH INTERNAL FLOOR PARTITION

J. MISSAOUI AND L. CHENG

Department of Mechanical Engineering, Laval University, Quebec, Canada G1K 7P4

(*Received* 4 *September* 1998, *and in final form* 5 *March* 1999)

Vibroacoustic analysis of a finite isotropic thin cylindrical shell with an internal floor partition is presented in the present paper. A general formulation is developed based on a variational approach in which the structural coupling between sub-structures is simulated using the artificial spring technique, while the acoustic field is computed by an integro-modal approach. For validation purposes, numerical results are compared with experimental data. Numerical analysis is performed to show the structural and acoustical effects of the floor on the internal pressure field. Further analysis is made to identify contributions of individual structural modes to sound radiation. The present paper illustrates how the two previously established methods (artificial spring technique and the integro-modal approach) can be combined into a vibroacoustic model in the prediction of the structural acoustic response of complex shaped cavities surrounded by structural boundaries.

1. INTRODUCTION

Structures based on cylindrical shell configurations have been extensively investigated in the literature. The study of the acoustic radiation of such structures is of considerable importance in many engineering applications, especially in the field of aerospace and ship engineering, where externally excited vibrating walls induce a significant internal sound field. A typical example is noise control inside airplane cabins. Due to the complexity of an airplane structure, simplified models are usually used to extract the overall tendency in terms of noise radiation to guide possible control actions.

One of the basic models is a cylindrical shell of either infinite or finite length [1–3]. More sophisticated models including different real-life components were also developed over the past few decades. Development of models considering the effects of rings [4], stiffeners [5], double walls [6] and bulkheads [7] have been an active research topic. A more realistic model requires us to take into consideration the floor. Compared to the cylindrical shells, the addition of the floor introduces more complex mechanical coupling. On top of this, the acoustic space inside the cabin no longer has a simple regular cylindrical shape. Due to both structural and

0022-460X/99/360101 + 23 $30.00/0

acoustic modifications, most methods based on modal decompositions can no longer be used. More powerful and efficient simulation models must therefore be developed.

An analytical development by Pope *et al.* [8, 9] has been used for shells with stiffeners, including floor and sidewall treatment. The model exploited the shell-floor configuration of Peterson and Boyd [10] with an extension which includes a smeared model for the stiffeners of Mikulas and McElman [11]. The acoustic modal characteristics of the irregular shaped cavity were calculated using the finite difference method. The model of Pope *et al.* [9] is regarded as a fairly complete model which incorporates a realistic configuration with a reasonable prediction accuracy of the noise levels in several tests. However, it is a complex and global model which is difficult to use to identify the effects of each individual component. Taking into account these complexities, Fuller [12] suggested a simplified model to study the structural influence of the floor on the sound transmission inside an infinite thin cylindrical shell coupled to a cylindrical shaped cavity. The floor was modelled by a series of periodic forces evaluated by a zero radial shell displacement condition. In doing this, the interaction between the floor and the enclosed acoustic space was neglected. Using this simplified model, it was noted that, in the plane of the excitation source, the structural effect of the floor is more significant at high frequencies.

Among works based on numerical methods, a recent study of Langley [13] used a hybrid approach combining the dynamic stiffness method for the structure and the boundary element method for the cavity. The author was interested in the problem of airborne noise transmission into an aircraft fuselage. Comparisons with experimental measurements, were limited to a purely cylindrical configuration. A structure-borne noise transmission prediction of a scale model fuselage was presented by Unruh and Dobosz [14] using the finite element method for up to 200 Hz. They showed that the number of elements required is a major computational difficulty when a detailed structural model is implicated. In another numerical model by Martin and Vignassa [15], the floor was treated as a rigid part and the internal walls covered with absorbing materials. The model included the bulkhead simulated as a flexible piston. Although these numerical methods are general and suitable for complex systems in the low-frequency range, it is clear that more simple and physical models permitting easy parametric studies are necessary.

In our previous work [16], a semi-analytical formulation has been developed on the free and forced vibrations of a shell-floor system. The mechanical coupling between sub-structures was modelled using the artificial spring technique. By allowing wide variations of the spring stiffness, different joint conditions can be simulated. As far as acoustic modelling is concerned, an integro-modal approach [17] for computing the acoustic properties of cavities of arbitrary shape has also been developed. The approach was based on a discretization of the total cavity into sub-cavities interconnected by virtual elastic membranes. Continuity of both the pressure and the pressure gradient at the boundaries of the interconnected regions was ensured by considering membranes with zero mass and stiffness.

The present work can be considered as an extension of the two previous works, aimed at carrying out a complete vibroacoustic analysis of the shell–floor-cavity

configuration. The following issues will be investigated. (1) Developing a general formulation which couples the structural model [16] with the acoustic model [17]. (2) Validating the developed model using experimental data. (3) Analyzing the acoustical and mechanical effects of the floor on the internal sound pressure and illustrating the sensitivity of the internal pressure to the floor connection. (4) Analyzing contributions of structural modes to the internal sound pressure. The proposed approach helps to give some physical insight into the physical system and offers a certain degree of flexibility in the design process.

2. DEVELOPMENT OF VIBROACOUSTIC MODEL

The structure to be investigated is composed of a thin finite cylindrical shell with an internal floor partition as shown in Figure 1. Both the shell and the floor are assumed to be homogeneous and isotropic. The co-ordinate system related to each main sub-structure is also defined in the same figure. Structural coupling between the shell and the floor is ensured using the artificial spring system for every permitted degree of freedom. For each junction, three translational springs (k_x, k_y, k_z) are introduced in the x, y_f, z_f directions, and for the rotational coupling, a torsion spring k_r is used. All spring stiffnesses are assumed to be uniformly distributed along the two junctions.

2.1. STRUCTURAL MODEL

The boundary conditions at the two ends are assumed to be simply supported. The displacement vector of the shell in the longitudinal, circumferential and radial directions is written as [16]

$$\begin{Bmatrix} u_s \\ v_s \\ w_s \end{Bmatrix} = \sum_{\alpha=0}^{1} \sum_{m=1}^{\infty} \sum_{n_s=0}^{\infty} c_{mn_s}^{\alpha} \begin{Bmatrix} a_{mn_s} \cos(n_s\,\theta - \alpha\tfrac{\pi}{2}) \cos(\tfrac{m\pi x}{L}) \\ b_{mn_s} \sin(n_s\,\theta - \alpha\tfrac{\pi}{2}) \sin(\tfrac{m\pi x}{L}) \\ 1 \cos(n_s\,\theta - \alpha\tfrac{\pi}{2}) \sin(\tfrac{m\pi x}{L}) \end{Bmatrix} e^{i\omega t}, \tag{1}$$

where $(a_{mn_s}, b_{mn_s}, 1)$ is the vector of a shear diaphragm condition with n_s and m being respectively the circumferential and longitudinal order, $\alpha = 0$ (or 1) denotes symmetric (or antisymmetric) modes and c_{mns}^{α}, are the coefficients to be determined.

For the floor, bending and in-plane motions are expanded over a trigonometric basis:

$$\begin{Bmatrix} u_f \\ v_f \\ w_f \end{Bmatrix} = \sum_{\alpha=0}^{1} \sum_{m=1}^{\infty} \sum_{n_f=0}^{\infty} \begin{Bmatrix} u_{mn_f}^{\alpha} \cos(\tfrac{n_f\pi}{b}\, y - \alpha\tfrac{\pi}{2}) \cos(\tfrac{m\pi x}{L}) \\ v_{mn_f}^{\alpha} \sin(\tfrac{n_f\pi}{b}\, y - \alpha\tfrac{\pi}{2}) \sin(\tfrac{m\pi x}{L}) \\ w_{mn_f}^{\alpha} \cos(\tfrac{n_f\pi}{b}\, y - \alpha\tfrac{\pi}{2}) \sin(\tfrac{m\pi x}{L}) \end{Bmatrix} e^{i\omega t}, \tag{2}$$

where n_f and m are, respectively, the transversal and longitudinal order, u_{mnf}^{α}, v_{mnf}^{α} and w_{mnf}^{α}, are the coefficients to be determined once the shell-floor are structurally coupled.

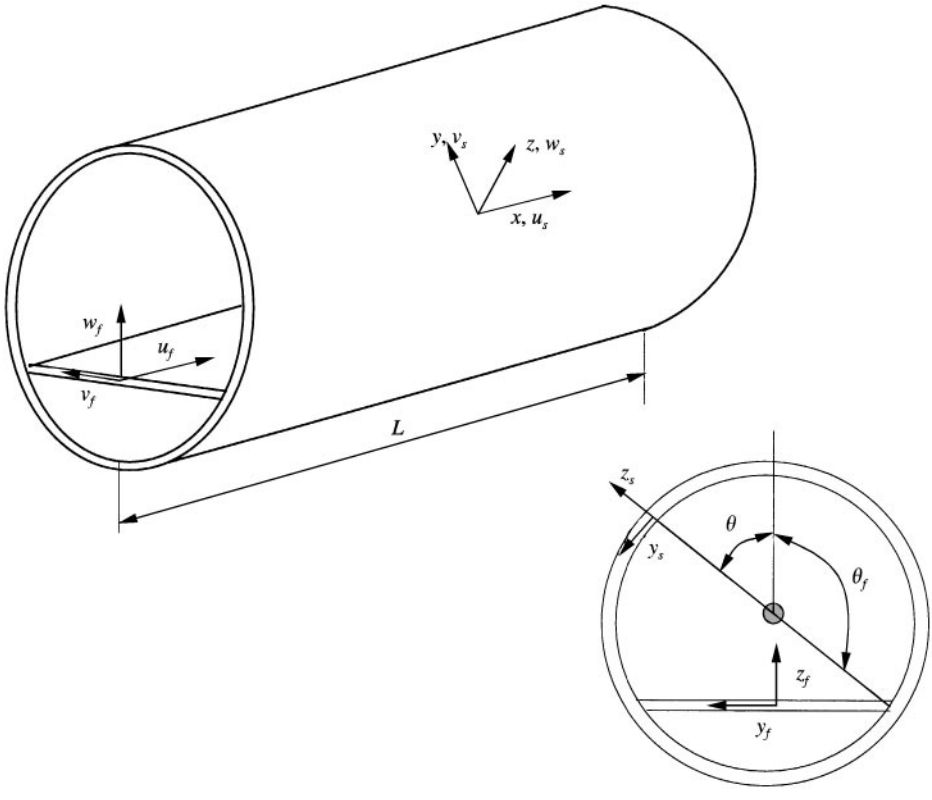

Figure 1. Shell–floor configuration.

The whole system is characterized using the classical Hamilton's principle, which needs the calculation of the kinetic and strain energy of the combined system, as well as the work done by the external driving forces and the fluid loading:

$$H = \int_{t_0}^{t_1} [T_c - \Pi_c + T_f - \Pi_f - E_k + \Pi_a + E_f] \, \mathrm{d}t, \tag{3}$$

where T_c, Π_c are the energies related to the shell, T_f, Π_f the energies related to the floor, Π_a, E_f the work done by the fluid and the external mechanical loading and E_k the strain energy stored in the artificial springs introduced at the longitudinal junctions.

The substitution of equations (1) and (2) in Hamilton's function (3) leads to expressions in terms of the unknown sets $c^{\alpha}_{mn_s}$, $u^{\alpha}_{mn_f}$, $v^{\alpha}_{mn_f}$ and $w^{\alpha}_{mn_f}$. Lagrange equations can then be used to extramilize Hamilton's function. The whole procedure yields the following governing equations of motion for the coupled system:

$$M_{mn_s} (\omega^2_{mn_s} - \omega^2) c^{\alpha}_{mn_s} + \sum_{n'_s} 2R^{1}_{mn_s n'_s \alpha} c^{\alpha}_{mn'_s}$$

$$+ \sum_{n'_f} [R^{12}_{mn_s n'_f \alpha} u^{\alpha}_{mn'_f} + R^{13}_{mn_s n'_f \alpha} v^{\alpha}_{mn'_f} + R^{14}_{mn_s n'_f \alpha} w^{\alpha}_{mn'_f}] = P^{\alpha}_{mn_s} - F^{\alpha}_{mn_s},$$

$$\sum_{n'_f} [k^u_{mn_f n'_f \alpha} - \omega^2 \, M^u_{n_f n'_f \alpha}] \, u^\alpha_{mn'_f} + \sum_{n'_f} k^{uv}_{mn_f n'_f \alpha} \, v^\alpha_{mn'_f} + \sum_{n'_s} R^{12}_{mn'_s n'_f \alpha} \, c^\alpha_{mn'_s} = 0,$$

$$\sum_{n'_f} [k^v_{mn_f n'_f \alpha} - \omega^2 \, M^v_{n_f n'_f \alpha}] \, v^\alpha_{mn'_f} + \sum_{n'_f} k^{uv}_{mn_f n'_f \alpha} \, u^\alpha_{mn'_f} + \sum_{n'_s} R^{13}_{mn'_s n'_f \alpha} \, c^\alpha_{mn'_s} = 0,$$

$$\sum_{n'_f} [k^w_{mn_f n'_f \alpha} - \omega^2 \, M^w_{n_f n'_f \alpha}] \, w^\alpha_{mn'_f} + \sum_{n'_s} R^{14}_{mn'_s n'_f \alpha} \, c^\alpha_{mn'_s} = - F^\alpha_{mn_f} - P^\alpha_{mn_f}, \tag{4}$$

In the above equations, ω_{mn_s} and M_{mn_s} are respectively the natural frequencies *in-vacuo* and the generalized modal mass of the shell, $k^w_{mn_f n'_f \alpha}$, $k^v_{mn_f n'_f \alpha}$, $k^u_{mn_f n'_f \alpha}$ and $k^{uv}_{mn_f n'_f \alpha}$ the generalized stiffness of the floor, $R^1_{mn_s n'_s \alpha}$ $R^{12}_{mn_s n'_f \alpha}$, $R^{13}_{mn_s n'_f \alpha}$ and $R^{14}_{mn_s n'_f \alpha}$ the contributions from the elastic attachment of the internal floor and $M^w_{n_f n'_f \alpha}$, $M^v_{n_f n'_f \alpha}$ and $M^u_{n_f n'_f \alpha}$ the generalized masses. The detailed calculation of these terms can be found in reference [16]. On the right-hand side of the equations (4), one can note the external mechanical force $F^\alpha_{mn_s}$, the internal mechanical loading $F^\alpha_{mn_f}$ and the fluid loading terms $P^\alpha_{mn_s}$, $P^\alpha_{mn_f}$ from the cavity. For the present model, the effect of fluid loading from outside and the contribution of the bulkhead are neglected.

2.2. ACOUSTICAL MODEL

The interior space is considered as an irregular-shaped cavity where variable separation techniques cannot be applied. The internal pressure is simulated using the integro-modal approach [17]. The method used a mixture of sub-cavities, of both regular and irregular shapes. The modal characteristics of regular sub-cavities are obtained analytically. For irregular ones, the procedure consists in enclosing the irregular sub-volume by envelopes or bounding sub-cavities, for which modal information is available. Since the natural modes of the irregular-shaped cavity are not known analytically,the modes of the bounding sub-cavities are used to perform the pressure decomposition and to obtain the Green's function.

In each sub-cavity, the internal pressure p_f can be calculated by transforming the Helmholtz equation into an integral from via the second Green's theorem,

$$p_f(r) = \int_{S_b} \left[G(r, r_0) \frac{\partial p_f(r_0)}{\partial \mathbf{n}} - p_f(r_0) \frac{\partial G(r, r_0)}{\partial \mathbf{n}} \right] \mathrm{d}s, \tag{5}$$

where $\mathbf{n}$ is the outward normal vector of the boundary surface S_b of the enclosure with volume V, $G(r, r_0)$ is Green's function corresponding to a transfer function obtained between an observation point (r) and the source (r_0). The construction of the function $G(r, r_0)$ for a Neumann boundary is based on the inhomogeneous Helmholtz equation with an infinite surface impedance [18]. Euler's equation of motion for a fluid particle can be combined with the continuity of the normal velocity component at the shell-sub-structure surfaces to establish the boundary conditions

$$\frac{\partial p_f}{\partial x} = 0, \quad x = 0, \quad x = L, \quad \forall \theta \in [-\theta_f, \theta_f], \quad \forall r \in [0, a],$$

$$\frac{\partial p_f}{\partial r} = -\rho_f \ddot{w}_s, \quad r = a, \quad \forall\theta \in [-\theta_f, \theta_f], \quad \forall x \in [0, L],$$

$$\frac{\partial p_f}{\partial z_f} = \rho_f \ddot{w}_f, \quad z_f = 0, \quad \forall y_f \in [-b/2, b/2], \quad \forall x \in [0, L], \tag{6}$$

where ρ_f is the fluid density, w_s and w_f are respectively the radial displacement of the shell and the flexural displacement of the floor.

Once the cavity of the shell–floor system is discretized into N sub-cavities, the integro-modal solution is obtained using either a direct method or an indirect one described as follows.

2.2.1. *Indirect method*

The indirect method uses the integro-modal formulation [17] to compute the modal characteristics of the whole cavity (natural frequencies, mode shapes and generalized mass). This information is then used to calculate the forced response.

The mode shapes $\Phi_{\bar{n}}^k$ in each sub-cavity k (Figure 2), computed using the integro-modal approach, are used as a basis of the expansion of the distributed pressure field:

$$p_f^k = \rho_f c_f^2 \sum_{\bar{n}} \frac{a_{\bar{n}}(t)}{\bar{\Lambda}_{\bar{n}}} \Phi_{\bar{n}}^k(r), \quad 1 \leqslant k \leqslant N, \tag{7}$$

where c_f is the speed of the sound in the internal medium, $\bar{n}$ are the modal indices of the cavity and $a_{\bar{n}}(t)$ the modal pressure amplitudes to be determine. $\bar{\Lambda}_{\bar{n}}$ is the generalized acoustic mass of order $\bar{n}$. Assuming that no absorbent boundary conditions are present and that the interior noise is due to arbitrary vibrating surfaces with structural modal co-ordinates $q_{\bar{m}}(t)$ (which is the whole set of the

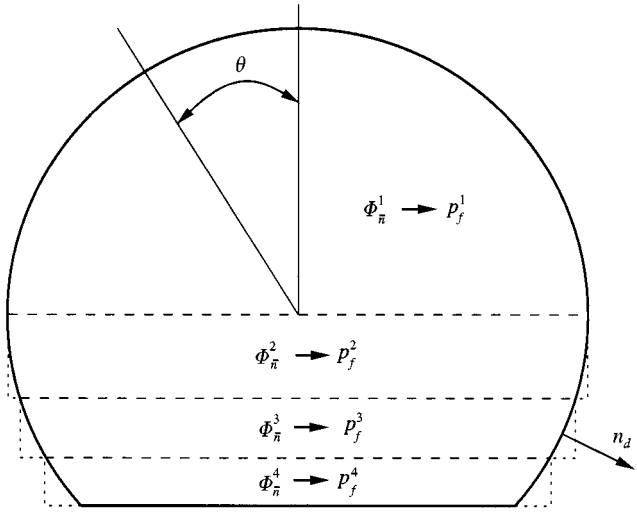

Figure 2. Discretization procedure using four sub-cavities.

structural unknows $c^{\alpha}_{mn_s}$, $u^{\alpha}_{mn_f}$, $v^{\alpha}_{mn_f}$ and $w^{\alpha}_{mn_f}$), the linear modal acoustic equation is given by

$$\ddot{a}_{\bar{n}} + \omega^2_{\bar{n}}\, a_{\bar{n}} + \sum_{k=1}^{N} \frac{A^k_f}{V} \sum_{\tilde{m}} \ddot{q}^k_{\tilde{m}}\, L^{k,k}_{\bar{n}\tilde{m}} - \frac{A^{N+1}_f}{V} \sum_{\tilde{m}} \ddot{q}^{N+1}_{\tilde{m}}\, L^{N,N+1}_{\bar{n}\tilde{m}} = 0, \tag{8}$$

where A^k_f is the area of the vibrating surface related to sub-cavity k and

$$L^{i,j}_{\bar{n}\tilde{m}} = \frac{1}{A^j_f} \int_{s^j} \Phi^i_{\bar{n}}(r_0)\, \psi^j_{\tilde{m}}(r_0)\, \mathrm{d}s^j \tag{9}$$

with $L^{ij}_{\bar{n}\tilde{m}}$ being the modal coupling coefficient between the structural mode of order $\tilde{m}$ and the cavity mode of order $\bar{n}$. This term characterizes the coupling in space between the two modes. The natural frequencies are obtained using the integro-modal approach for the calculation of the 2D natural frequencies and the condition given by the separation of variables applied to the longitudinal geometry:

$$\omega^2_{\bar{n}} = \omega^2_i + c^2_f\, (q\pi/L)^2, \tag{10}$$

where q is the acoustical longitudinal order and ω_i is a 2-D natural frequency of order i, L is the length of the cavity.

2.2.2. *Direct method*

Compared to the indirect method, the direct approach does not require calculations of modal characteristics of the real cavity. In each sub-cavity, however, the acoustic equation is written using analytical mode shapes of its bounding sub-cavity (called envelope), whilst structural motion of each membrane is characterized by assigning zero mass and stiffness. The forced response of the system is then computed.

The internal pressure in each sub-cavity is obtained by using a modal basis of the bounding sub-cavity or envelope

$$p^k_f = \rho_f\, c^2_f \sum_{n} \frac{a^k_n(t)}{\Lambda^k_n}\, \phi^k_n(r), \quad \forall k \in [1, N], \tag{11}$$

where Λ^k_n, ϕ^k_n are respectively the generalized acoustic mass and the eigenfunction of the bounding sub-cavity k.

Using the integro-modal approach, the substitution of equation (11) in equation (5) leads to the following modal acoustic equations inside each sub-cavity:

$$\ddot{a}^k_n + \omega^2_{n,k}\, a^k_n = -\frac{A^k_f}{V^k} \sum_{\tilde{m}} \ddot{q}^k_{\tilde{m}}\, L^{k,k}_{n\tilde{m}} - \frac{A^{k+1}_f}{V^k} \sum_{\tilde{m}} \ddot{q}^{k+1}_{\tilde{m}}\, L^{k,k+1}_{n\tilde{m}}, \quad k = 1;$$

$$\ddot{a}^k_n + \omega^2_{n,k}\, a^k_n + \frac{c^2_f}{V^k} \sum_{n'} \frac{a^k_{n'}}{\Lambda^k_{n'}} \int_{S^k} \phi^k_{n'} \frac{\partial \phi^k_n}{\partial \mathbf{n}^k_d}\, \mathrm{d}s = \frac{A^{2k-2}_f}{V^k} \sum_{\tilde{m}} \ddot{q}^{2k-2}_{\tilde{m}}\, L^{k,2k-2}_{n\tilde{m}}$$

$$- \frac{A^{2k-1}_f}{V^k} \sum_{\tilde{m}} \ddot{q}^{2k-1}_{\tilde{m}}\, L^{k,2k-1}_{n\tilde{m}} - \frac{A^{2k}_f}{V^k} \sum_{\tilde{m}} \ddot{q}^{2k}_{\tilde{m}}\, L^{k,2k}_{n\tilde{m}}, \quad \forall k \in [2, N-1];$$

$$\ddot{a}_n^k + \omega_{n,k}^2 a_n^k + \frac{c_f^2}{V^k} \sum_{n'} \frac{a_{n'}^k}{\Lambda_{n'}^k} \int_{S^k} \phi_{n'}^k \frac{\partial \phi_n^k}{\partial \mathbf{n}_d^k} \, \mathrm{d}s = \frac{A_f^{2k-2}}{V^k} \sum_{\tilde{m}} \ddot{q}_{\tilde{m}}^{2k-2} \, L_{n\tilde{m}}^{k,2k-2}$$

$$- \frac{A_f^{2k-1}}{V^k} \sum_{\tilde{m}} \ddot{q}_{\tilde{m}}^{2k-1} \, L_{n\tilde{m}}^{k,2k-1} - \frac{A_f^{2k}}{V^k} \sum_{\tilde{m}} \ddot{q}_{\tilde{m}}^{2k} \, L_{n\tilde{m}}^{k,2k}, \quad k = N; \tag{12}$$

where the modal acoustic characteristics $\omega_{n,k}$, $\Lambda_{n'}^k$ and volume V^k are those of the bounding sub-cavity k; $\mathbf{n}_d^k$ is the outward normal vector of sub-cavity k. The continuity equation between two adjacent sub-cavities is

$$\sum_n \frac{a_n^k}{\Lambda_n^k} L_{n\tilde{m}}^{k,k} - \sum_n \frac{a_n^{k+1}}{\Lambda_n^{k+1}} L_{n\tilde{m}}^{k+1,k} = 0, \quad \forall k \in [1, N-1]; \quad L_{n\tilde{m}}^{i,j} = \frac{1}{A_f^j} \int_{s^j} \phi_n^i(r_0) \, \psi_{\tilde{m}}^j(r_0) \, \mathrm{d}s^j. \tag{13}$$

$L_{n\tilde{m}}^{i,j}$ is again the acoustoelastic coupling between virtual membrane modes and acoustical models of the bounding sub-cavity.

2.3. SOUND-STRUCTURE INTERACTION

2.3.1. Direct method

Using the direct method, the final matrix equations based on equations (4) and (12) can be written as

$$\begin{bmatrix} K_{SS}(\omega) & 0 & K_{SF} \\ 0 & 0 & C_{FF} \\ B_{FS}(\omega) & B_{FM}(\omega) & A_{FF}(\omega) \end{bmatrix} \begin{Bmatrix} U^s \\ U^m \\ P \end{Bmatrix} = \begin{Bmatrix} F_{SS} \\ 0 \\ 0 \end{Bmatrix}, \tag{14}$$

where U^s, U^m and P are respectively the unknowns related to the structural components, virtual membranes and acoustical vectors. K_{SS} is the dynamic stiffness matrix of the structural system. K_{SF} is the fluid–structure coupling matrix. C_{FF} is the continuity matrix across artificial membranes. B_{FS} and B_{FM} are matrices obtained using various coefficients of the acoustoelastic coupling. A_{FF} contains the acoustical mass and stiffness matrices. F_{SS} is the vector related to the mechanical excitation force.

2.3.2. *Indirect method*

Using the indirect method, the matrix system based on equations (4) and (8) is written as

$$\begin{bmatrix} \hat{K}_{SS}(\omega) & \hat{K}_{SF} \\ \hat{B}_{FS}(\omega) & \hat{A}_{FF}(\omega) \end{bmatrix} \begin{Bmatrix} U^s \\ P \end{Bmatrix} = \begin{Bmatrix} \hat{F}_{SS} \\ 0 \end{Bmatrix}. \tag{15}$$

Compared with the direct method, the system to be solved is of reduced size, since modal characteristics of the whole cavity (natural frequency, generalized mass and mode shape) should be calculated *a priori* using the integro-modal approach.

The vibroacoustic parameters are chosen to characterize the structural and acoustical responses of the system. In fact, at each excitation frequency, the motion

of the each sub-structure is characterized by the quadratic velocity for the shell and the floor defined by

$$\langle V_s^2 \rangle = \frac{\omega^2}{4} \sum_{\alpha=0}^{1} \sum_{m=1}^{\infty} \sum_{n_s=0}^{\infty} \varepsilon_{n_s}^{-1}\, c_{mn_s}^{\alpha} (c_{mn_s}^{\alpha})^*, \tag{16}$$

$$\langle V_f^2 \rangle = \frac{\omega^2}{4b} \sum_{\alpha=0}^{1} \sum_{m=1}^{\infty} \sum_{n_f=0}^{\infty} \sum_{n'_f=0}^{\infty} \beta_{n_f n'_f}^{\alpha}\, w_{mn_f}^{\alpha} (w_{mn'_f}^{\alpha})^*, \tag{17}$$

where $\in_{n_s}$ is 1 (if $n_s = 0$) or 2 (if $n_s \neq 0$), $(c_{mn_s}^{\alpha})$ and $(w_{mn'_f}^{\alpha})^*$ are respectively the complex conjugate of $c_{mn_s}^{\alpha}$ and $w_{mn'_f}^{\alpha}$. In equation (17), the coefficient $\beta_{n_f n'_f}^{\alpha}$ is given by

$$\beta_{n_f n'_f}^{\alpha} = \int_{y=-b/2}^{y=b/2} \cos\left(\frac{n_f \pi}{b}\, y - \alpha \frac{\pi}{2}\right) \cos\left(\frac{n'_f \pi}{b}\, y - \alpha \frac{\pi}{2}\right) \mathrm{d}y. \tag{18}$$

For the cavity, an average quadratic pressure is defined as

$$\langle p_f^2 \rangle = \frac{1}{2V} \int_V p_f(M)\, p_f^*(M)\, \mathrm{d}v, \tag{19}$$

where p_f^* is the complex conjugate of p_f at an arbitrary point M in the cavity.

3. RESULTS AND DISCUSSIONS

In all calculations reported hereafter the shell and the floor are assumed to have the same thickness and the same material properties. The used data are $\rho_s = 7860\ \mathrm{kg/m^3}$, $\nu = 0{\cdot}3$, $E = 2{\cdot}07E11\ \mathrm{N/m^2}$, $L = 1{\cdot}209$ m, $a = 0{\cdot}254$ m, $h_s = h_f = 3{\cdot}2 \times 10^{-3}$ m, $\theta_f = 131^\circ$. Unless specified, the shell–floor attachment is assumed to be rigid with ($\bar{k} = 10^9$) and the stiffness parameters are normalized with respect to the flexural rigidity of the structure. The speed of sound and the air density are respectively $c_f = 343$ m/s and $\rho_f = 1{\cdot}2\ \mathrm{kg/m^3}$. The input load is a unit point force acting either at the external surface of the shell ($x = 0{\cdot}31$ m, $\theta = 90^\circ$) or inside the cavity on the floor ($x = 0{\cdot}31$ m, $y_f = 0{\cdot}10$ m). Structural damping models are used for both the structure and the cavity. In both cases, loss factors are set to be 5×10^{-3}. In all calculations, the acoustic model is based on the direct method using one bounding cylindrical cavity.

The truncation of the infinite series, used in both the structural displacement and sound pressure decomposition, to a limited number of terms is a computational restriction. The general procedure to find a suitable series truncation is aimed at assuring the desired accuracy in the resulting solutions. This requirement can be achieved by increasing the number of terms used in the expansions in equations (1), (2), (7) or (11) until convergence is achieved in the frequency range of interest. In numerical simulations, a single cylindrical cavity was used as the envelop. During the calculations a careful convergence study was carried out for the shell–floor-cavity response in the case of an excitation on the external surface of the shell. A typical results is presented in Figure 3, where there curves are compared using different maximum orders (longitudinal, circumferential and radial) or (5, 5, 5), (8, 8, 8) and (10, 15, 10) for the acoustical response. The maximum structural terms used in equations (1) and (2) are truncated to 10 longitudinal terms, 15

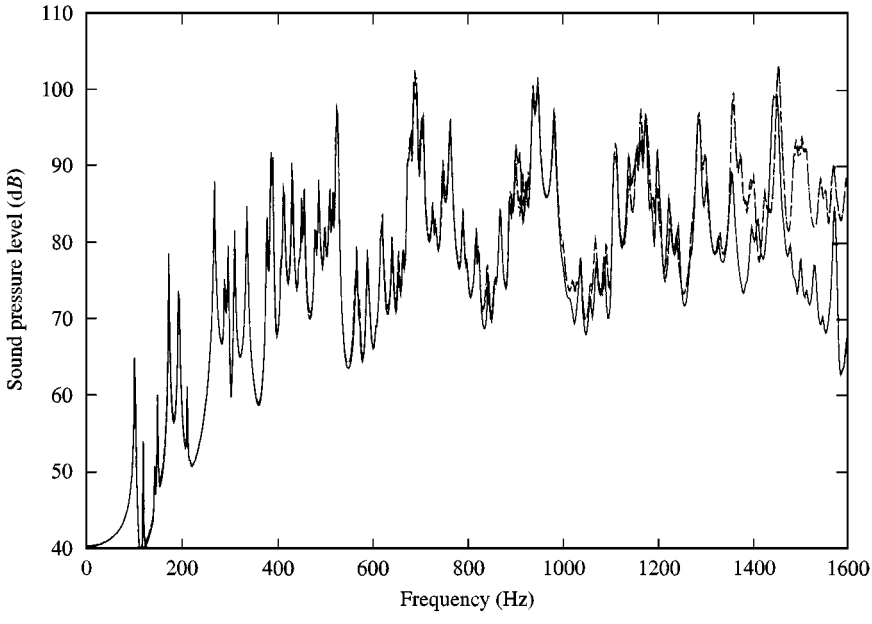

Figure 3. Convergence curves of the internal pressure: ———, (5, 5, 5); – – –, (8, 8, 8); –. –. –, (10, 15 10).

circumferential terms for the shell, and 18 terms for the floor including the in-plane motion ($n_m^* = 10$, $n_s^* = 15$, $n_w^* = 8$, $n_u^* = n_v^* = 5$). It can be observed that good convergence is obtained for the three different bases of truncation up to 800 Hz. Beyond this frequency limit, a (8, 8, 8) truncation is sufficient to ensure a good convergence up to 1600 Hz. A systematic convergence analysis has also been performed in the case where the full coupling between the cavity and the surrounding sub-structures is considered [19]. It was noted that fluid loading effect of the acoustic cavity on the structure is relatively weak. Slight differences can only be noticed above 1000 Hz in our case. In following calculations, the fluid loading due to the cavity below the floor partition is therefore neglected.

3.1. EXPERIMENTAL VALIDATION

In order to validate the proposed vibroacoustic model, experimental tests were performed to assess the method using a cavity simulating an aircraft cabin. In numerical simulations, the terms used are respectively (8, 8, 8) for the cavity and (10, 15, 8, 5, 5) for the structure.

The experimental set-up and instrumentation used are illustrated in Figure 4. The cavity was formed by a steel cylinder with a floor welded to the inner shell skin. The interior space of concern was the volume above the floor. Two steel end caps of 0·0254 m thick were used to form the rigid acoustic boundaries. The test cylinder had an internal diameter of 0·504 m and was 1·1684 m long. The floor was made of steel as the cylinder, and was located at an angle θ_f of 131°. Two $\frac{1}{2}$ in microphones

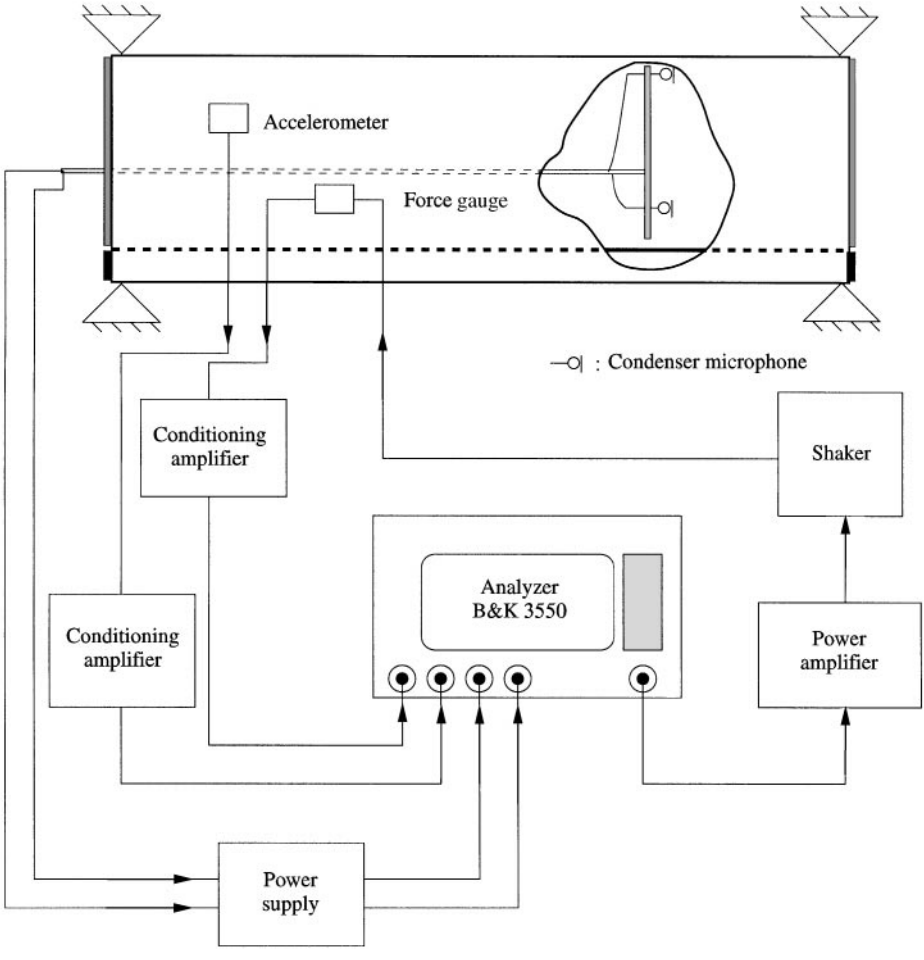

Figure 4. Experimental set-up.

were placed inside the cavity supported by a thin tube along the cylinder centerline. The tube could rotate and be moved along the centerline to get any desired measurement point. A point force was produced by a shaker and applied on the outside of the shell surface. Accelerometers and force transducers were used to measure the structural response and the excitation force. Measured data were treated using a multi-channel B&K 3550 FFT Analyzer. Comparisons between predicted and measured results are performed in terms of transfer functions.

A comparison between the predicted and measured displacement/force transfer functions averaged over six measuring points, made over both a narrow and $\frac{1}{3}$ octave band is given in Figures 5 and 6 respectively. The six points were chosen at positions on the surface of the shell defined by angular positions of 50 and 70° and longitudinal positions at 0·24 m, 0·48 and 0·72 m. It can be seen that the agreement between the vibroacoustic model and the experimental data is generally satisfactory. The fact that so many resonances occur over the measured frequency

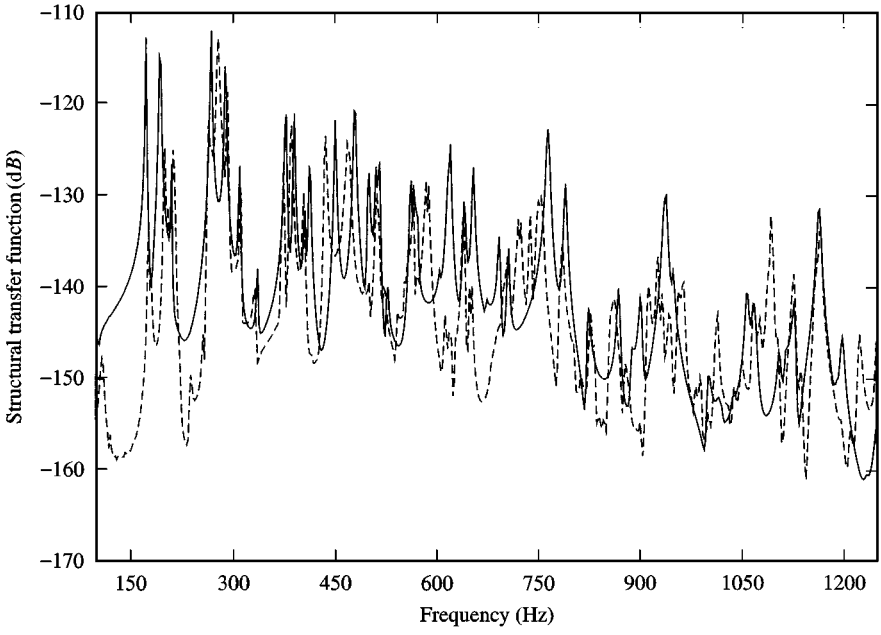

Figure 5. Predicted and measured structural response in narrow band: ———, predicted; – – –, measured.

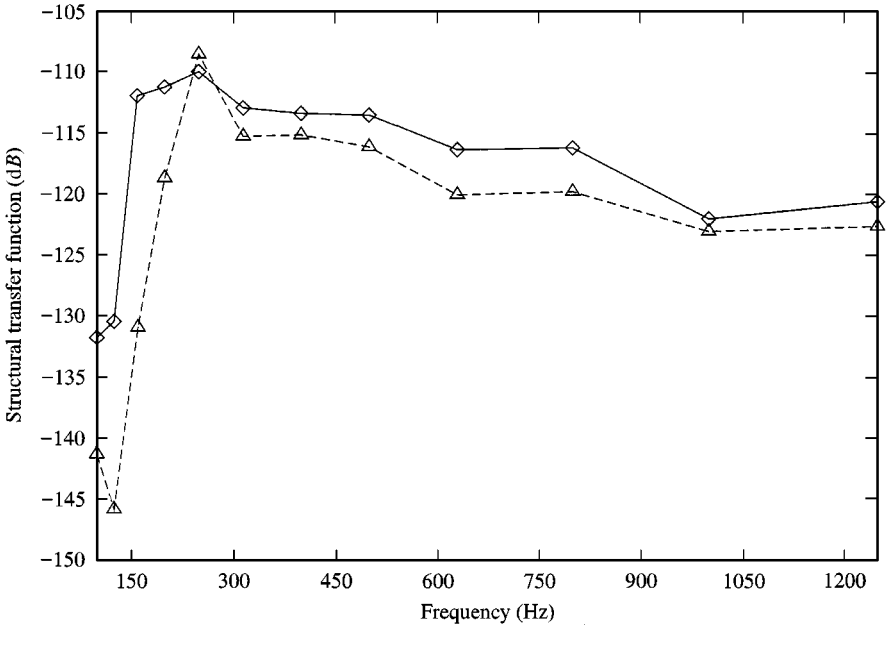

Figure 6. Predicted and measured structural response in $\frac{1}{3}$ octave band: ◇——◇, predicted; –Δ–Δ–, measured.

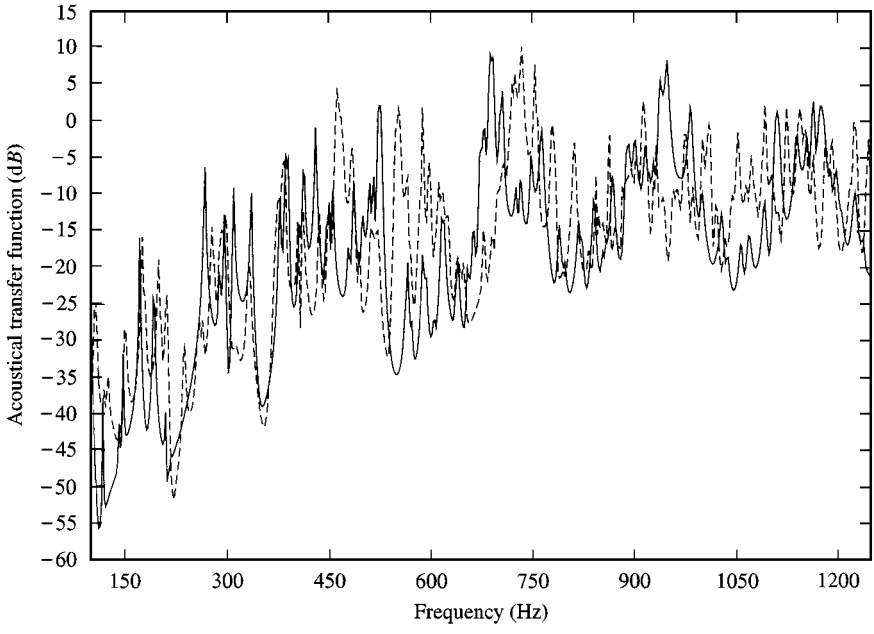

Figure 7. Predicted and measured acoustical response in narrow band: ——, predicted; – – –, measured.

zone illustrates the complexity of the dynamics of the structure investigated. However, one notices local differences in both the levels and the resonant frequencies. This is certainly due to diverse several factors such as welding, lack of symmetry, differences in the experimental structural boundary conditions, etc. It should be noted that in the $\frac{1}{3}$ octave band, the discrepancy between the two curves does not exceed 5 dB beyond 200 Hz.

Using the same configuration, comparisons were also made of the response of the cavity using sound pressure/force transfer functions. A total of 18 measurement points inside the cavity was used [angular position: (20, 40 and 60°), radial position: (0·56 × radius, 0·19 × radius), longitudinal position: (0·8567, 0·5567 and 0·2567 m)]. The comparison in the narrow band, between experiment and simulation, is illustrated in Figure 7. The response of the two signals in the third octave band is illustrated in Figure 8. Generally speaking, the tendencies observed indicate an acceptable agreement between the two models. However, while following the evolution of the two curves in the narrow band, one notes differences in the levels in the resonant frequencies. As a whole, the proposed model seems to be powerful enough to predict the general tendency of the response of the system.

3.2. EFFECTS OF THE FLOOR

Regrding the effects of the floor, numerical results are presented herein in terms of the average sound pressure level inside the cavity and the quadratic velocity of

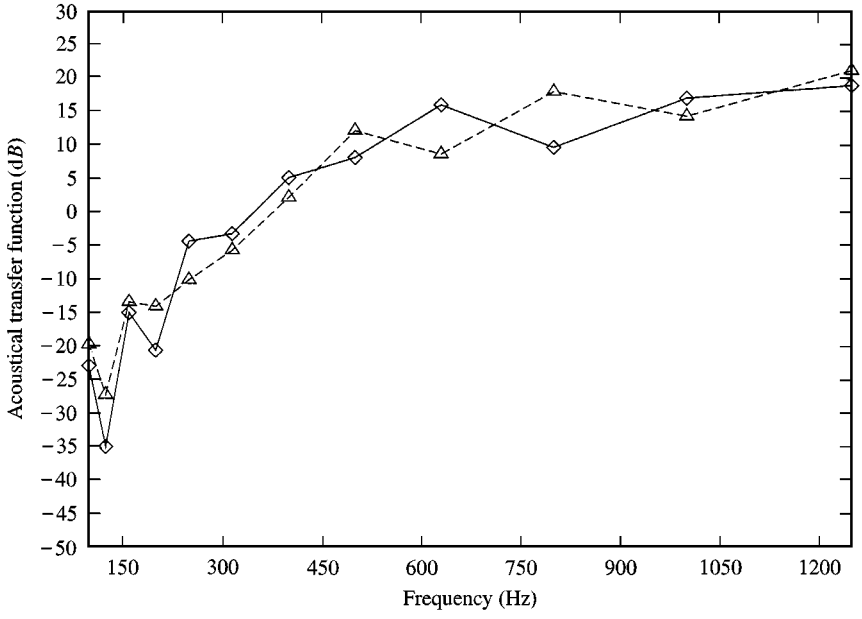

Figure 8. Predicted and measured acoustical response in $\frac{1}{3}$ octave band: ◇—◇, predicted; –Δ–Δ–, measured.

the shell and the floor. The quadratic velocity is represented in terms of dB referenced to 5×10^{-8} m/s.

Previous work [16] has identified the existence of three types of mode shapes. The first type is a floor dominated by a strong floor motion. The second type is essentially a shell mode in which a slight deformation of the floor and a dominate shell motion are observed. The third type is a coupled mode in which the two sub-structures vibrate with comparable levels. It was also noticed that when the shell is directly excited, the vibration levels for both sub-structures are of the same order of magnitude at both the low and middle frequencies, indicating a strong coupling between them. It is therefore interesting to investigate the contribution of each component (floor and shell) in terms of acoustic radiation. This is illustrated in Figure 9, where the individual contributions of the shell and that of the floor to the internal sound pressure are compared. One notices that the floor radiation can attain a comparable level to that of the shell at several low frequencies. Generally speaking, however, although the floor certainly affects the dynamics of the shell, its direct radiation seems to be negligible. Consequently, the sound pressure inside the cavity seems to come mainly from the shell radiation.

From a pratical point of view, although the excitations usually apply to the shell, an excitation of the floor can be an interesting configuration for a better understanding of the system. It may also be of practical use in ship structure analysis, where embarked equipment on board can generate strong vibrations and noise. To this end, a point force was applied to the floor at ($x = 0.31$ m, $y_f = 0.10$ m). Figure 10 compares the quadratic velocity levels of both shell and the

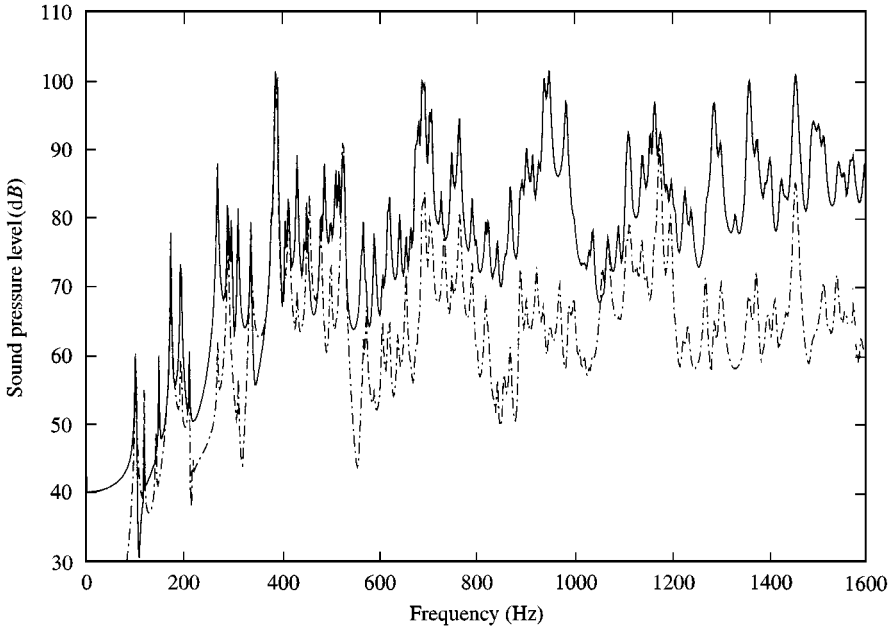

Figure 9. Sound pressure level ratiated by shell and floor with excitation on the shell: ———, shell; – · – · –, floor.

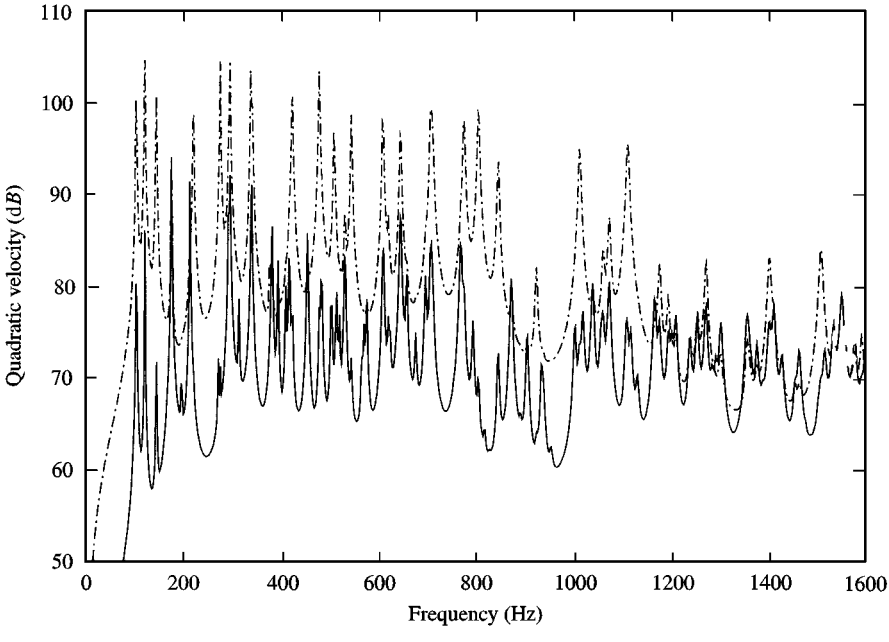

Figure 10. Structural response with the floor subjected to a unit point force: ———, shell; – · – · –, floor.

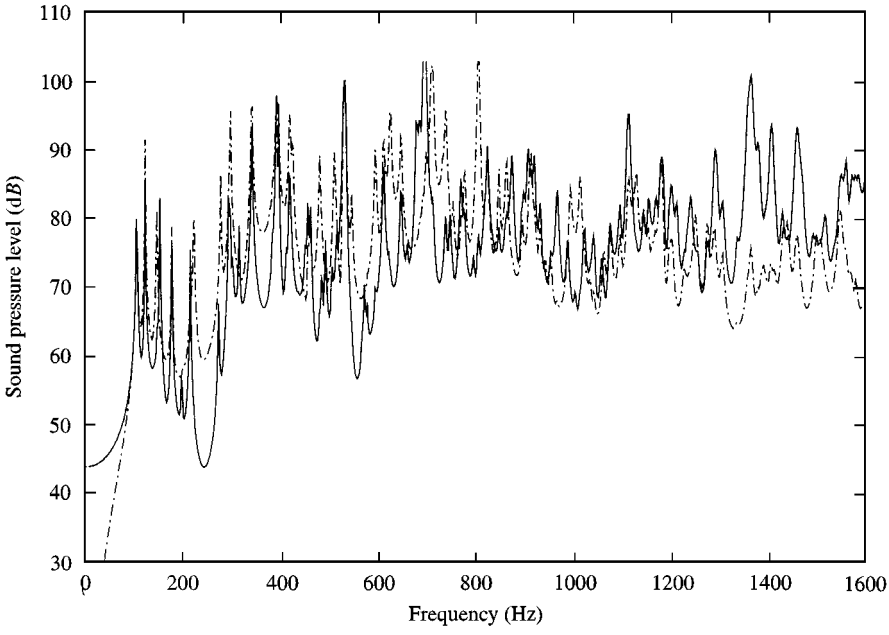

Figure 11. Sound pressure level ratiated by shell and floor with excitation on the floor: ———, shell; – · – · –, floor.

floor. Being directly excited, the floor manifests a dominating role in the structural response. Resonances correspond to motions dominated by floor controlled modes and coupled modes. The mechanical energy transmitted to the shell across the junctions seems to be comparable to that of the floor at high frequencies. Sound pressure contributions of each components are compared in Figure 11. It should be noted that, despite the relatively weak vibration level of the shell, the latter still remains a strong sound radiator. Although not directly excited, the shell plays a significant role in terms of sound radiation.

Numerical simulations have also been performed to illustrate the effects of the joint conditions between the shell and the floor on teh generated cavity noise. As has been poinhted out, by setting different values for the stiffness parameter varying from 0 to infinity, both limit cases (rigid and free) and elastic cases can simulated.

An example with a hinged joint is also given. Figure 12 compares the sound pressures levels inside the cavity with two different joint conditions: rigid and hinged connnection ($k_r = 0$). It can be seen that the connection via rotation does not basically change the general trend of the overall pressure levels of the cavity. Figures 13 and 14 illustrated comparisons between the vibration level of each sub-structure in the case of rigid and pinned connection. It can be noticed that the effects are not significant on the shell response, even if changes can be observed on the locations of resonant peaks. In addition, the curves presented in Figure 14 show that this kind of connection is significant for the floor. Indeed, a flexible connection via rotation shifted the first resonance towards the low frequencies. Generally

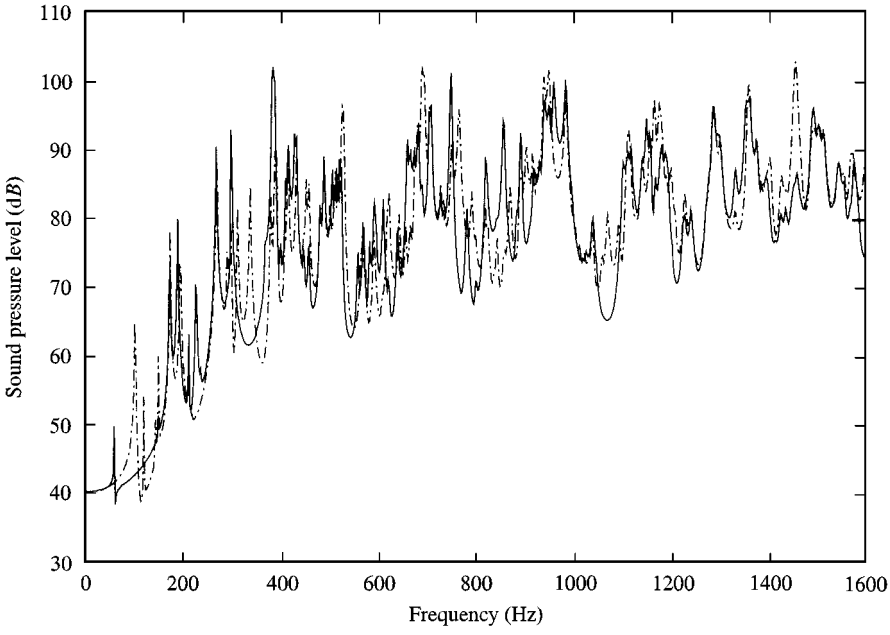

Figure 12. Acoustic effects of a rigid and hinged connection: ———, hinged; – · – · –, rigid.

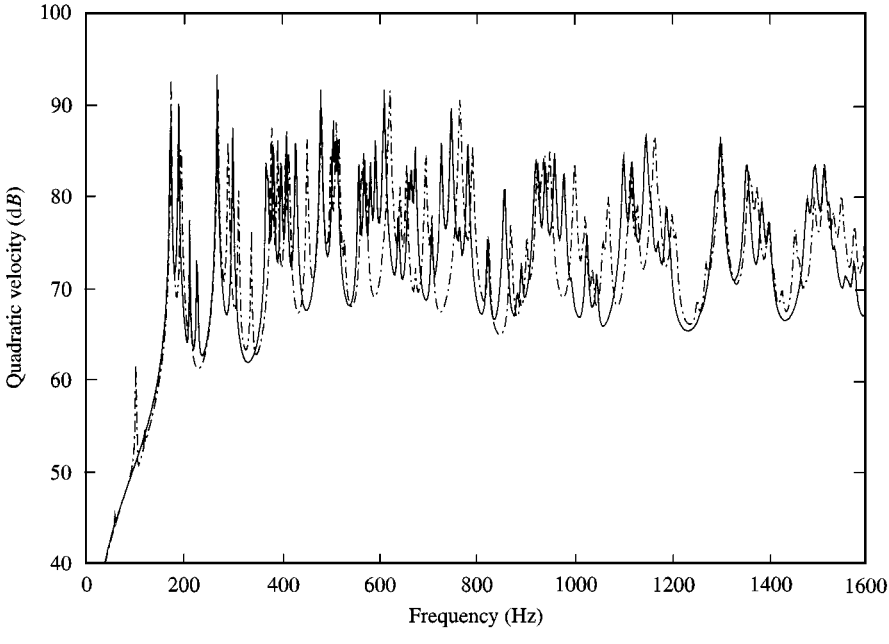

Figure 13. Effects of a rigid and hinged connection on the shell vibration: ———, hinged; – · – · –, rigid.

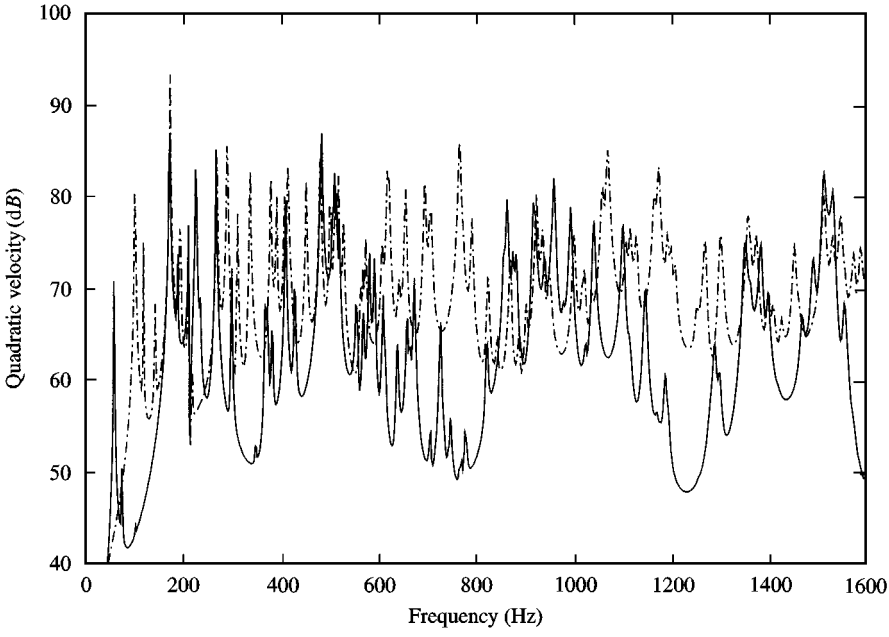

Figure 14. Effect of a rigid and hinged connection on the floor vibration: ———, hinged; – · – · –, rigid.

speaking, the vibration level is decreased for most frequency ranges. Details concerning the elastic cases can be found in reference [19].

As mentioned before, the use of purely cylindrical configurations in the investigation of noise transmission in aircraft fuselages usually provides much simpler models. Fuller and Jones [20] have demonstrated that the circumferential modal response is the dominant factor in the problem of noise transmission. The structual modification introduced by the floor has a frequency-dependent stiffening effect on the radial motion at the floor attachment points. Consequently, the sound pressure level associated with structural vibration is also changed. In addition, the insertion of the floor also changes the acoustic modes by converting a cylindrical cavity into a less irregular shape. An analysis was performed to separate the structural effect from the acoustical one in order to isolate the contribution of each individual modification.

The acoustic effect of the floor was simulated using a rigid floor without any structural attachment to the shell. This was carried out by cutting off the terms related to the floor motion and the connecting springs in the equations. The comparison with the standard configuration is made in Figure 15. A decrese in the sound pressure level can be observed at low frequencies which can be attributed to the elimination of the floor mode in this region. The acoustical effect of the floor is obvious above this zone. Since, as already illustrated in Figure 9, the floor radiation is almost negligible in this region compared to that of the shell, the difference noticed in Figure 15 must be due to the acoustic effect (change of acoustic modes) of the floor.

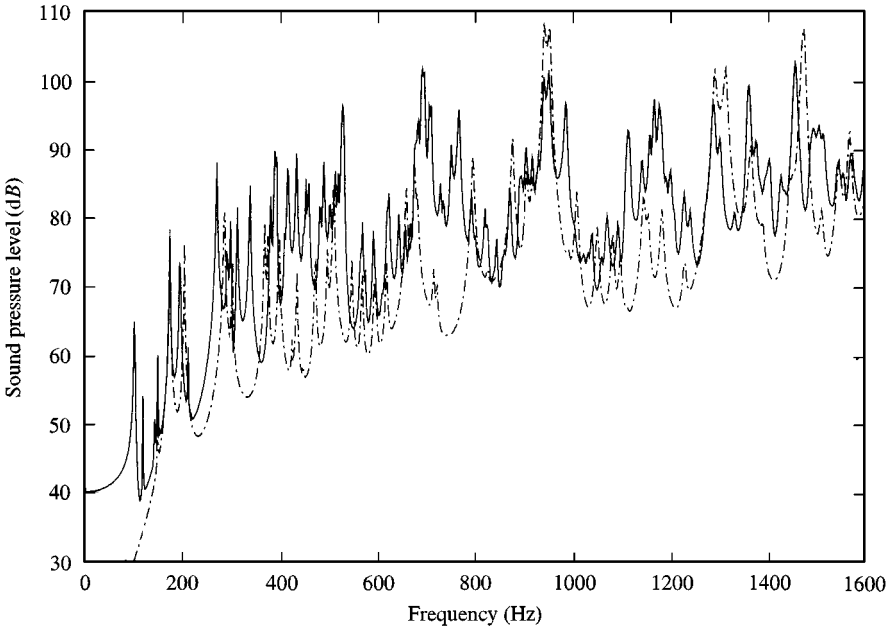

Figure 15. Acoustic effect of the floor: ———, standard configuration; – · – · –, modified configuration.

On the other hand, the structural effect of the floor is simulated by considering it as an integral part of the structure while being transparent from the acoustic point of view. The sound pressure in the upper part of the cylindrical cavity is compared with that of the standard configuration in Figure 16. One can notice that the structural influence is frequency dependent. It remains however, less significant than the acoustic effects mentioned above. These conclusions are consistent with the experimental results of Fuller and Jones [21, 22] obtained for a number of discrete frequencies with a simplified aircraft fuselage model. The present analysis provides a more detailed description of the phenomena covering a wide spectrum of frequencies. It can thus be concluded that the presence of the floor affects the internal sound field basically via the modifications of the acoustic cavity rather than its direct structural effect.

3.3 MODAL RADIATION EFFICIENCY

In typical problems of cavity–structure interaction, structural modes do not contribute in the same way to the radiated sound. Any control noise actions should be taken on the most radiating modes. It is therefore interesting to highlight the contribution of each structural mode to the internal radiation of the vibrating sub-structures. Using the present formulation, an analysis is performed using several representative structural modes. The procedure consists of solving the eigenvalue problem of equation (4) without the fluid and the mechanical

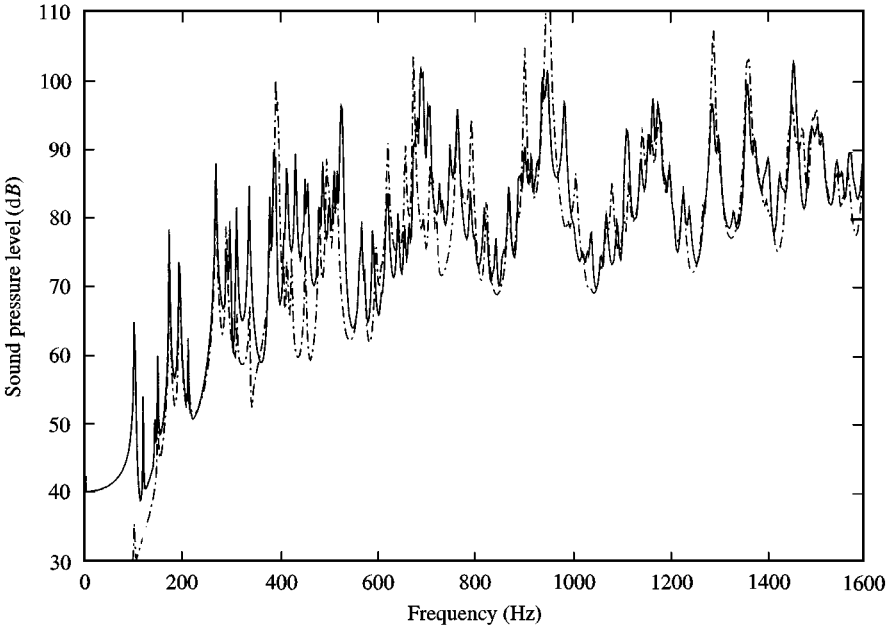

Figure 16. Structural effect of the floor: ———, standard configuration; – · – · –, modified configuration.

excitations. Substituting the structural unknowns in equation (12) from the resulting eigenvectors makes it possible to calculate the acoustic modal amplitudes and to deduce the internal pressure and other vibroacoustic parameters. As pointed out in a previous publication [23], the commonly used radiation efficiency in free field radiation problems in no longer suitable for the cavity problems, since in this case, the radiated power becomes the power absorbed by the cavity. A new parameter $\bar{\sigma}$ using the radiated potential acoustic energy is defined as

$$\bar{\sigma} = 10 \log \left(\frac{E_{ac}}{E_{cg}} \right), \tag{20}$$

where E_{ac} is the potential acoustic energy in the cavity due to the vibration of the surrounding walls, and E_{cg} the total kinetic energy of these walls. These two energy quantities are defined respectively by

$$E_{ac} = \frac{1}{2} \int_V \frac{p_f^2}{\rho_f c_f^2} \, \mathrm{d}v, \quad E_{cg} = \frac{1}{2} \rho_s h_s A_f^c \langle V_s^2 \rangle + \frac{1}{2} \rho_f h_f A_f^f \langle V_f^2 \rangle. \tag{21}$$

$\bar{\sigma}$ is a dimensionless parameter which is calculated for each selected structural mode of show its sound contribution with respect to frequencies. Figure 17 illustrates the modal radiation efficiency of four selected structural modes (with $m = 1$) whose deformations are plotted in Figure 18. It is noted that peaks which are present in the spectrum correspond to the natural frequencies of the cavity to which the structural modes are coupled. The first mode considered is totally controlled by

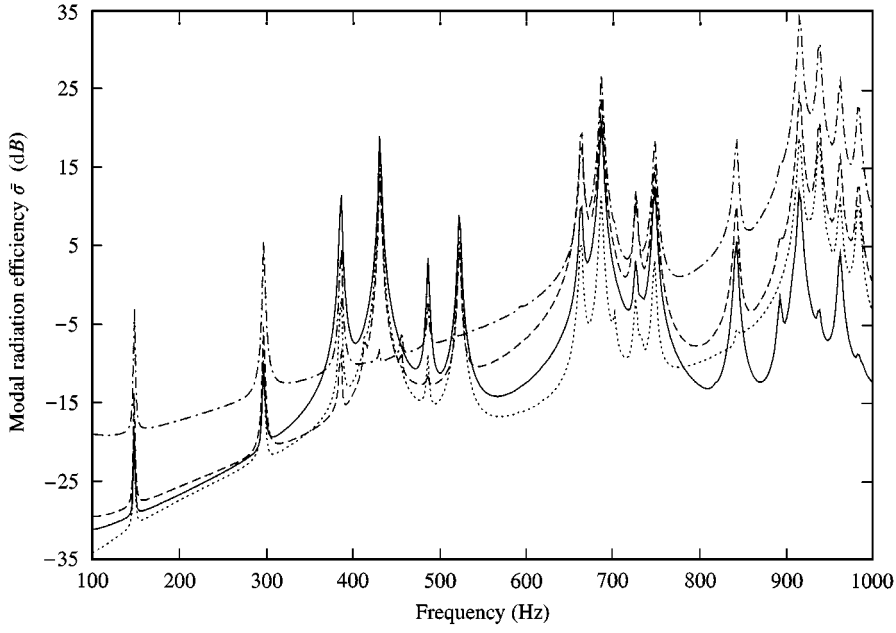

Figure 17. Modal radiation efficiency of four typical structural modes: ———, mode 1; – – –, mode 2; – · – · –, mode3; . . . . , mode 4.

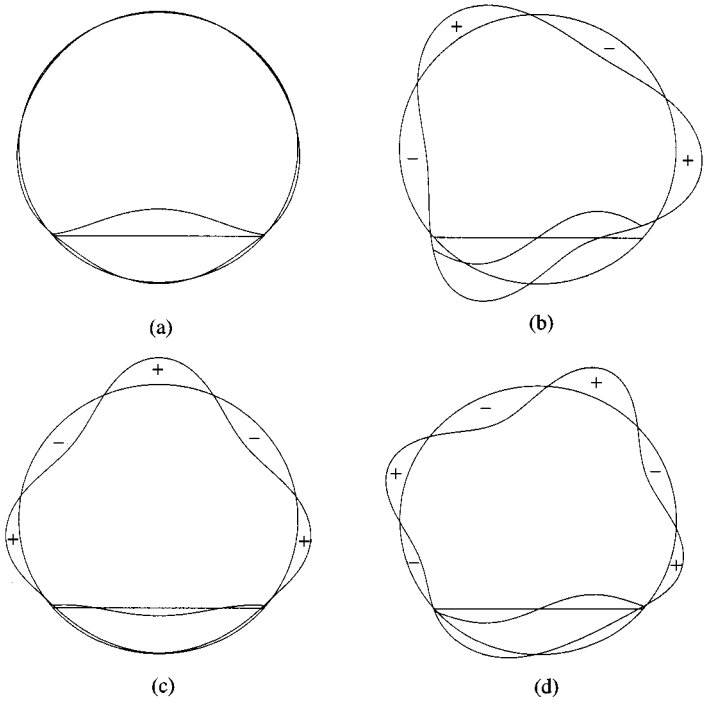

Figure 18. Mode shapes of the selected structural modes: (a) mode 1, (b) mode 2, (c) mode 3, (d) mode 4.

floor motion, whose radiation efficiency is strong in the middle frequency range. It is interesting to compare the three other modes, all involving strong shell motion. Of the three modes, mode 3 seems to be the most radiating over a large frequency range. One of the plausible explanations may be given by noticing the wave front of each mode as illustrated in Figure 18. In the part of the shell above the floor, modes 2 and 4 have the same number of positive and negative cells, so that there may be a cancellation process in the circumferential direction. Mode 3 however, has three positive cells and tow negative ones so that the cancellation effect may be less effective. In addition, it can be noticed that the wave number is smaller for mode 2 than for mode 4. The results seem to indicate that modes with mismatched positive and negative cells and those having smaller wave numbers in the circumferential direction are susceptible to radiate more strongly. Verifications were also made using a series of other modes with $m = 1$, the aforementioned observation seems to be valid in most cases. It should be stressed that the modal efficiency of each mode strongly depends on the cavity configuration and is certainly a complex matter. Further analysis using other configurations is therefore required for a better understanding of the phenomena.

4. CONCLUSION

This paper presented a vibroacoustic study of a shell–floor-cavity system. Two previously established methods (Artificial Springer technique and the integro-modal approach) were combined into a complete vibroacoustic model. Experiments were carried out to assess the established model. Although further improvements are still needed, numerical predictions using the present formulation seem to agree reasonably well with experimental data. The method is shown to be powerful enough to predict the vibroacoustic response of the shell–floor-cavity system.

Numerical analyses were performed to highlight the structural and acoustic effects of the floor on the sound field. It was noted that in any case, shell vibration plays an important role in the sound radiation into the cavity. When the excitation is applied to the shell, the floor becomes a very weak sound radiator. In this case, the effect of the floor is limited to changes in shape of the cylindrical acoustic cavity, leading to significant differences in terms of sound level compared to what would have been predicted using a purely cylindrical shell configuration. When the excitation is applied to the floor, however, shell radiation can still remain strong. Using the present configuration, analyzes of the modal radiation efficiency were also performed. Results revealed a possible cancellation process between cells of opposite phase in circumferential direction.

REFERENCES

1. L. R. Koval 1976 *Journal of Sound and Vibration* **48**, 265–275. On sound transmission into a thin cylindrical shell under flight conditions.
2. C. R. Fuller 1986 *Journal of Sound and Vibration* **109**, 141–156. Analytical model for investigation of interior noise characteristics in aircraft with multiple propellers including synchrophasing.

3. D. A. Bofilios and C. S. Lyrintzis 1991 *AIAA Journal* **29**, 1193–1201. Structure-borne noise transmission into cylindrical enclosures of finite extent.
4. B. Laulagnet and J. L. Guyader 1990 *Journal of Sound and Vibration* **138**, 173–191. Sound radiation by finite cylindrical ring stiffened shells.
5. M. T. Chang and R. Vaicaitis 1982 *Journal of Sound and Vibration* **85**, 71–84. Noise transmission into semi-cylindrical enclosures thought discrete curves panels.
6. E. H. Dowell 1980 *Journal of Aircraft* **17**, 690–699. Interior noise studies for single and double walled cylindrical shells.
7. L. Cheng 1994 *Journal of Sound and Vibration* **174**, 641–654. Fluid-structural coupling of a plate-ended cylindrical shell: vibration and internal sound field.
8. L. D. Pope and J. F. Wilby 1977 *Journal of the Acoustical Socieity of America* **62**, 906–911. Band limited power flow into enclosures I.
9. L. D. Pope, E. G. Wilby, C. M. Willis and W. H. Mayes 1983 *Journal of Sound and Vibration* **89**, 371–417. Aircraft interior noise models: stiffened structures, and cabin acoustics with floor partition.
10. M. R. Peterson and D. E. Boyd 1978 *Journal of Sound and Vibration* **60**, 45–62. Free vibrations of circular cylindders with longitudinal, interior partitions.
11. M. R. Mikulas and J. A. McElman 1965 *NASA TN D*-3010. On free vibrations of eccentrically stiffened cylindrical shells and flat plates.
12. C. R. Fuller 1987 *Journal of Aircraft* **24**, 731–736. Structural influence of the cabin floor on sound transmission into aircraft: analytical investigations.
13. R. S. Langley 1993 *Journal of Sound and Vibration* **163**, 207–230. A dynamic stiffness/boundary element method for the prediction of interior noise levels.
14. J. F. Unruh and S. A. Dobosz 1988 *Journal of Vibration, Acoustics, Stress and Reliability in design* **110**, 226–233. Fuselage structural-acoustic modelling for structure-borne interior noise transmission.
15. V. Martin and P. Vignassa 1994 *Journal of Sound and Vibration* **176**, 307–332. Numerical vibroacoustic modelling of aircraft for the active acoustic control of interior noise.
16. J. Missaoui, L. Cheng and M. J. Richard 1996 *Journal of Sound and Vibration* **190**, 21–40. Free and forces vibration of a cylindrical shell with a floor partition.
17. J. Missaoui and L. Cheng 1997 *Journal of the Acoustical Society of America* **101**, 3313–3321. A combined integro-modal approach for predicting acoustic properties of irregular-shaped cavities.
18. P. M. Morse and H. Feshbach 1953 *Methods of Theoretical Physics*, Vol. II, New York; McGraw–Hill.
19. J. Missaoui 1998 *Ph. D. dissertation, Laval University, Quebec*. Étude vibor-acoustique d'un système coque-plancher-cavité avec application à un fuselage simplifiè.
20. J. D. Jones and C. R. Fuller 1984 *AIAA Paper* 84–2370. Noise control characteristics of synchrophasing: an experimental investigation.
21. J. D. Jones 1987 *Ph. D. thesis, Virginia, USA*. A study of active control techniques for noise reduction in an aircraft fuselage model.
22. J. D. Jones and C. R. Fuller 1988 *Journal of Aircraft* **25**, 882–889. Influence of a floor on sound transmission into an aircraft fuselage model.
23. L. Cheng and J. Nicolas 1992 *Journal of the Acoustical Society of America* **91**, 1504–1513. Radiation of sound into a cylindrical enclosure from a point driven end plate with general boundary conditions.